# Evaluation of surface integrity when drilling Inconel 718 through experimental measurement and finite element analysis

*By* Amrifan Saladin Mohruni

WORD COUNT 5405
TIME SUBMITTED 13-APR-2023 03:40PM
PAPER ID 98675266

The International Journal of Advanced Manufacturing Technology
https://doi.org/10.1007/s00170-021-08354-y

ORIGINAL ARTICLE

# Evaluation of surface integrity when drilling Inconel 718 through experimental measurement and finite element analysis

Mohammad Lotfi[1] · Ali Akhavan Farid[2] · Javad Akbari[1] · Safian Sharif[3] · Amrifan Saladin Mohruni[4]

Received: 21 July 2021 / Accepted: 6 November 2021


**Abstract**
Surface integrity is one of the important parameters affecting the quality and functionality of mechanical components. This paper presents an investigation on effect of drilling parameter on the surface integrity of Inconel 718 through a combination of experimental and simulation works. The machining responses that are determined through the experimental work include microhardness, microstructure changes, and surface roughness. The average grain size of the microstructure of the workpiece is estimated by using a simulation model. The experimental and simulation results show that higher spindle speed facilitates the formation of white layer near the machined surface and decreases the average grain size. Furthermore, it is observed that the surface finish deteriorates with an increase in feed rate.

**Keywords** Microstructure · Simulation · Surface integrity · Inconel 718

## 1 Introduction

Some alloys are considered as difficult-to-cut materials where nickel-based alloys fall into this category. Owing to the characteristics such as poor thermal conductivity, rapid strain hardening, and high strength, the machining of these materials is difficult [1, 2]. In the meantime, other characteristics such as high resistance in creep, oxidation, and corrosion had attracted these materials to be used in aerospace industry for the components of aircraft engine [3]. Inconel 718 is one of the nickel-based superalloys which encounters difficulties when undergoes machining process. Tool wear conditions and surface integrity are the two crucial factors that need to be addressed when machining Inconel 718 [4].

✉ Javad Akbari
akbari@sharif.edu

[1] School of Mechanical Engineering, Sharif University of Technology, 14588-89694 Tehran, Iran

[2] Department of Mechanical, Materials and Manufacturing Engineering, University of Nottingham Malaysia Campus, 43500 Semenyih, Malaysia

[3] School of Mechanical Engineering, Faculty of Engineering, Universiti Teknologi Malaysia, 81310 Johor Bahru, Johor, Malaysia

[4] Mechanical Engineering Department, Sriwijaya University, 30662 Inderalaya, South Sumatra, Indonesia

It is well understood that the service lifetime and the quality of the components are dependent on the surface properties [5]. Severe damage due to cracking, fatigue, and creep starts from the surface of the components which largely depends on the surface quality. Thus, in the machining of mechanical components, the surface integration needs to be considered [6]. Microhardness, microstructure (grain size), and surface roughness are classified as surface integrity [7]. Accordingly, Azim et al. [8] investigated the effect of cutting parameters on surface integrity of nickel-based super alloy in microdrilling process. It was reported that an increase in feed value caused thrust and radial forces to be increased. Sharman et al. [9] conducted a series of experiments to evaluate the surface roughness in drilling of Inconel 718. They expressed that the roughness values were produced in the range of 1 to 1.5 $\mu$m. In two other studies [10, 11], it was mentioned that microstructure and chemical composition of Inconel 718 were the main factors influencing the surface integrity and cutting process.

Apart from the experimental work, a detailed approach is needed to make a correlation between microstructure changes (grain size) and surface integrity of Inconel 718. Since it cannot be sufficiently done just by conducting experimental studies, therefore finite element (FE) simulation method could be a useful approach to predict the grain sizes of Inconel 718 at different cutting conditions. Different models were used by researchers to predict the grain size

Published online: 11 January 2022

**Table 1** The chemical compositions of Inconel 718

| Element | Ni | Cr | Mo | Fe | Nb | Ti |
|---|---|---|---|---|---|---|
| Component (wt. %) | ≥ 54 | 18 | 3 | 18.5 | 5 | 1 |

variations in simulation work. Rotella and Umbrello [12] and Jafarian et al. [13] used Zener-Hollomon model to estimate the grain size of titanium alloy and Inconel 718, respectively, during turning simulation. Denguir et al. [14] and Ding and Shin [15] simulated the microstructure changes by using Estrin-Kim model. In two other studies, Arısoy and Özel [16, 17] used Johnson-Mehl-Avrami-Kolmogorov (JMAK) model to simulate the grain size of Inconel 100 and titanium alloy. They reported that the model could appropriately predict the grain size variations. Bai et al. [18] also used JMAK model during turning of Ti-6Al-4V alloy where the simulation was carried out in two dimensions. Lotfi et al. [19] predicted the microstructure changes in 3D simulation of turning process by using JMAK model. They showed that the turning process reduced the grain sizes.

With respect to the above descriptions, this study is undertaken to investigate the surface integrity of Inconel 718 during drilling process by conducting a series of experimental measurement tests (such as microhardness, microstructure, and surface roughness) and by development of a simulation model to calculate the grain size variations. One of the difficulties of grain size measurement of Inconel 718 is the low reproducibility of results, particularly, when the cutting conditions are close to each other; therefore, the innovation of this study is the use of an FE model to precisely predict the grain size variations at different cutting conditions.

## 2 Experimental procedures

Experimental trials were conducted on a MAHO MH 700S CNC machine. The workpiece material was Inconel 718 with 105 mm × 105 mm× 18 mm dimension. The chemical composition of Inconel 718, which is used in this study, is given in Table 1. An uncoated tungsten carbide (WC) twist drill with 6 mm in diameter was selected for the drilling operation. Figure 1 shows the experimental equipment for the drilling trials. Cutting forces were measured by using a KISTLER dynamometer (9443B type) and a Handy-surf tester model (E-35A) was used to measure the surface roughness of the wall of the drilled holes. To evaluate the microstructure of the drilled holes wall of Inconel 718, the specimens were sectioned along the hole axis (as seen in Fig. 1). Then, the specimens were mounted in cold method by using low viscosity epoxy resin. Wet ground was applied to prepare the surface of the specimens and was repeated by different silicon carbide papers (from 100 to 4000 grit sizes). After the polishing process, the specimens were etched by using an electrolytic etching device (Buehler). The etching process was conducted for 15 sec to using a stainless steel cathode with 3% of sulfuric acid at electrical condition of 6 Volts and temperature of 24 °C. The microstructure of the specimens were observed under an optical microscope. Figure 2 illustrates the as-received microstructure of Inconel 718. The average

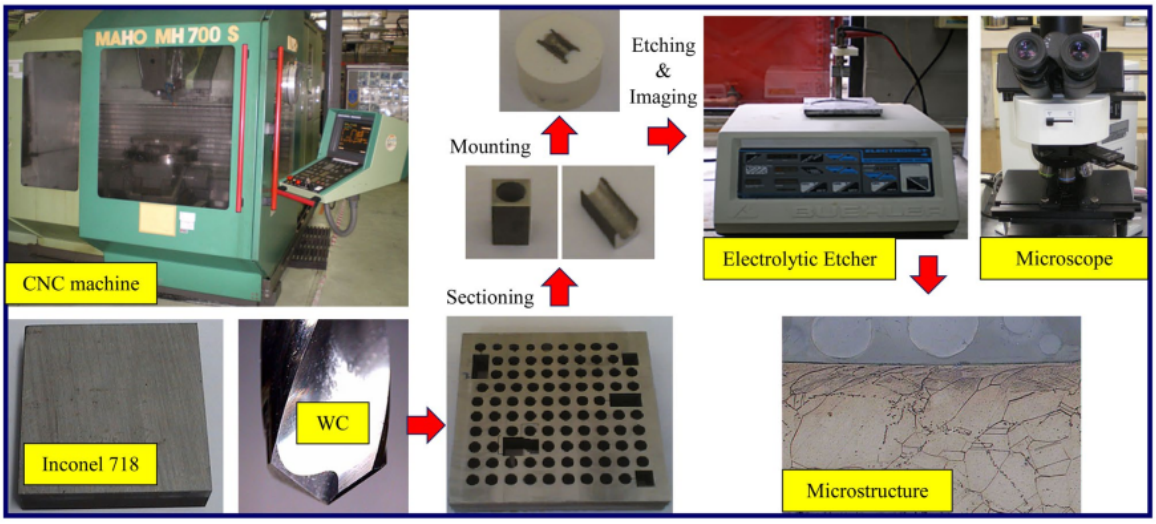


**Fig. 1** Experimental procedures

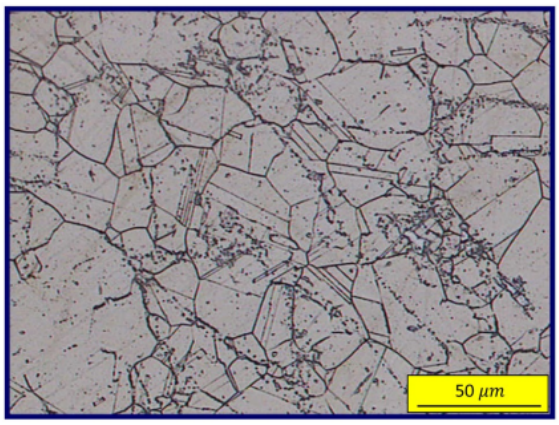


**Fig. 2** As-received microstructure of Inconel 718

grain size was approximately 43 $\mu$m and was used for the simulation study, as it is explained in the next section. Drilling experiments were under four different feeds and spindle speeds, as given in Table 2. Depth of cut was kept constant at 18 mm which equal to workpiece thickness (the process was through drilling).

## 3 Simulation modeling

To simulate the drilling process, the CAD models of the workpiece and the drill bit were drawn and CAD files were transferred to the DEFORM 3D software. The workpiece was meshed by 50,000 tetrahedron mesh elements. A mesh window was also applied at the cutting zone (due to large deformation) where the mesh size was 0.00001 compared to the mesh elements located out of the window (Fig. 3). The drill bit was meshed by 13000 mesh elements. In accordance with Fig. 3, the rotary and feed motions were applied on the drill bit and workpiece, respectively. The properties of the workpiece material (Inconel 718) and the drill bit (WC) are given in Table 3.

**Table 2** Experimental runs

| Run number | Feed (mm/rev) | Spindle speed (rpm) |
|---|---|---|
| 1 | 0.05 | 424 |
| 2 | 0.08 | 424 |
| 3 | 0.10 | 424 |
| 4 | 0.12 | 424 |
| 5 | 0.05 | 690 |
| 6 | 0.08 | 690 |
| 7 | 0.10 | 690 |
| 8 | 0.12 | 690 |
| 9 | 0.05 | 955 |
| 10 | 0.08 | 955 |
| 11 | 0.10 | 955 |
| 12 | 0.12 | 955 |
| 13 | 0.05 | 1220 |
| 14 | 0.08 | 1220 |
| 15 | 0.10 | 1220 |
| 16 | 0.12 | 1220 |

Johnson-Cook flow stress model ($\tilde{\sigma}$) (Eq. 1), Cockcroft-Latham damage criterion ($D$) (Eq. 2), and hybrid sticking-sliding friction model (Eq. 3) were used to consider the material behavior during deformation, damage, and drill-chip contact zone, respectively.

$$\tilde{\sigma} = \left[A + B\left(\bar{\varepsilon}\right)^{n}\right]\left[1 + Cln\left(\frac{\dot{\bar{\varepsilon}}}{\dot{\bar{\varepsilon}}_0}\right)\right]\left[1 - \left(\frac{T - T_e}{T_m - T_e}\right)^{m}\right] \quad (1)$$

$$D = \int_0^{\varepsilon_f} \sigma^* d\bar{\varepsilon} \quad (2)$$

$$\begin{cases} \tau_f = mkif\, \mu\sigma_n \geq mk, (Sticking) \\ \tau_f = \mu\sigma_n if\, \mu\sigma_n < mk, (Sliding) \end{cases} \quad (3)$$

In Eq. (1), the constant parameters are A = 450 MPa, B = 1700MPa, C = 0.017, $n = 0.65$, and $m = 1.3$ which represent the yield strength, hardening modulus, strain rate sensitivity, strain-hardening, and thermal softening exponent, respectively. $T_e$, $T_m$, and $T$ are the temperature of environment, melting temperature, and the working temperature, respectively. Finally, $\dot{\bar{\varepsilon}}_0$, $\bar{\varepsilon}$, and $\dot{\bar{\varepsilon}}$ are the reference of plastic strain rate, the equivalent strain, and the plastic strain rate, respectively [22]. In Eq. (2), $\sigma^*$, $\varepsilon_f$, and $\bar{\varepsilon}$ are effective stress, fracture strain, and effective strain [23]. The critical damage criterion is shown by $D$ which is equal to 500 MPa [20]. In Eq. (3), $m$ is the sticking friction (equal to 1), $\mu$ is the sliding friction (equal to 0.65), $\sigma_n$ is the normal stress, $k$ is the shear flow stress of working material, and $\tau_f$ is the frictional shear stress. The values were obtained by using an iteration process considering the cutting forces [24].

JMAK model has been utilized in order to simulate the microstructure changes during the drilling process. That being the case, the average grain size, which was defined based on the experimental measurement, was used as the initial grain size for the simulation work which was 43 $\mu$m for Inconel 718. Furthermore, the constant parameters of JMAK model were extracted from previous researches (listed in Table 4) [25]. The model consists of the following equations that was divided into three categories: 1, peak strain (Eqs. 4 and 5); 2, dynamic recrystallization kinetics (Eqs. 6 and 7); and 3, dynamic recrystallization grain size (Eqs. 8 and 9):

$$\varepsilon_c = a_2\varepsilon_p \quad (4)$$

**Fig. 3** Simulation setup

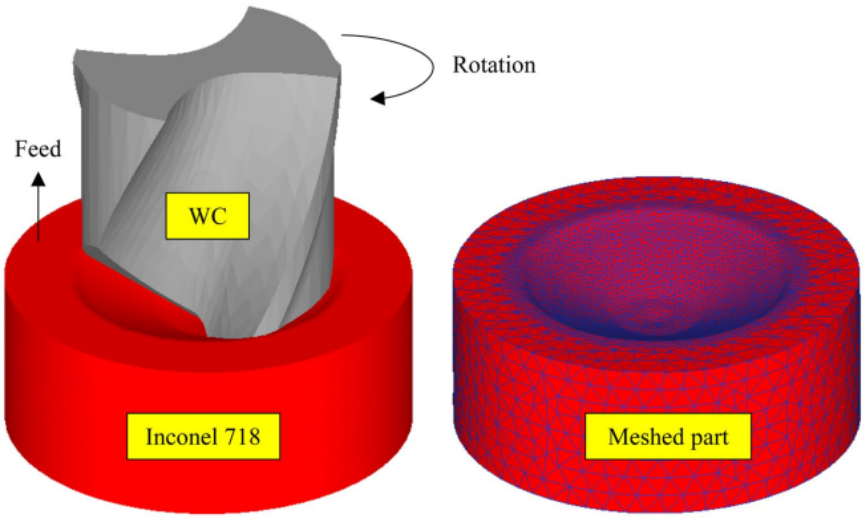


$$\varepsilon_p = a_1 d_0^{h_1} \dot{\varepsilon}^{m_1} e^{\left(\frac{Q_1}{RT}\right)} + c_1 \tag{5}$$

$$X_{DR_x} = 1 - exp\left[-\beta_d \left(\frac{\varepsilon - a_{10}\varepsilon_p}{\varepsilon_{0.5}}\right)^{k_d}\right] \tag{6}$$

$$\varepsilon_{0.5} = a_5 d_0^{h_5} \varepsilon^{n_5} \dot{\varepsilon}^{m_5} e^{\left(\frac{Q_5}{RT}\right)} + c_5 \tag{7}$$

$$d_{DR_x} = a_8 d_0^{h_8} \varepsilon^{n_8} \dot{\varepsilon}^{m_8} e^{\left(\frac{Q_8}{RT}\right)} + c_8 \tag{8}$$

$$d_{avg} = d_0\left(1 - X_{DR_x}\right) + d_{DR_x} X_{DR_x} \tag{9}$$

where $\varepsilon_c$ is the critical strain, $\varepsilon_p$ is the peak strain, $DR_x$ is the dynamic recrystallization, $T$ is the temperature,$\dot{\varepsilon}$ is the strain rate, $\varepsilon$ is the strain,$\varepsilon_{0.5}$ is the strain in 50% recrystallization, $Q$ is the activation energy, and $d_0$ is the initial grain size [19]. The rest of parameters are constant parameters related to the JMAK model.

**Table 3** The properties of Inconel 718 (workpiece) and WC (drill bit) [20, 21]

| Properties | Unit | Inconel 718 | WC |
|---|---|---|---|
| Thermal conductivity | W/M/°C | 10.3 | 59 |
| Specific heat | J/Kg/°C | 362 | 1500 |
| Thermal expansion | $10^{-6}$/°C | 13 | 5 |
| Elastic modulus | GPa | 217 | 650 |
| Poisson's ratio | - | 0.3 | 0.25 |
| Density | g/cm$^3$ | 8.22 | 15.7 |
| Melting temperature | °C | 1400 | 2870 |

## 4 Results and discussions

### 4.1 Model evaluation

Simulation of the drilling process was implemented in 1000 steps for each particular run number, as listed in Table 2, and the 6 steps of the simulation run are illustrated in Fig. 4. In this figure, chip formation and microstructure changes are observed during drilling process.

**Table 4** The parameters of JMAK model for Inconel 718 [25]

| Models | Parameter | Value |
|---|---|---|
| Peak strain | $a_1$ | 0.004659 |
| | $n_1$ | 0 |
| | $m_1$ | 0.1238 |
| | $Q_1$ | 49520 |
| | $c_1$ | 0 |
| | $a_2$ | 0.83 |
| $DR_x$ kinetics | $a_5$ | 294 |
| | $h_5$ | 340 |
| | $n_5$ | 512 |
| | $m_5$ | 593 |
| | $Q_5$ | 600 |
| | $c_5$ | 0 |
| | $\beta_d$ | 0 |
| | $k_d$ | 0 |
| | $a_{10}$ | 0 |
| $DR_x$ grain size | $a_8$ | 48500000000 |
| | $h_8$ | 0 |
| | $n_8$ | − 0.41 |
| | $m_8$ | − 0.028 |
| | $Q_8$ | − 240000 |
| | $c_8$ | 0 |

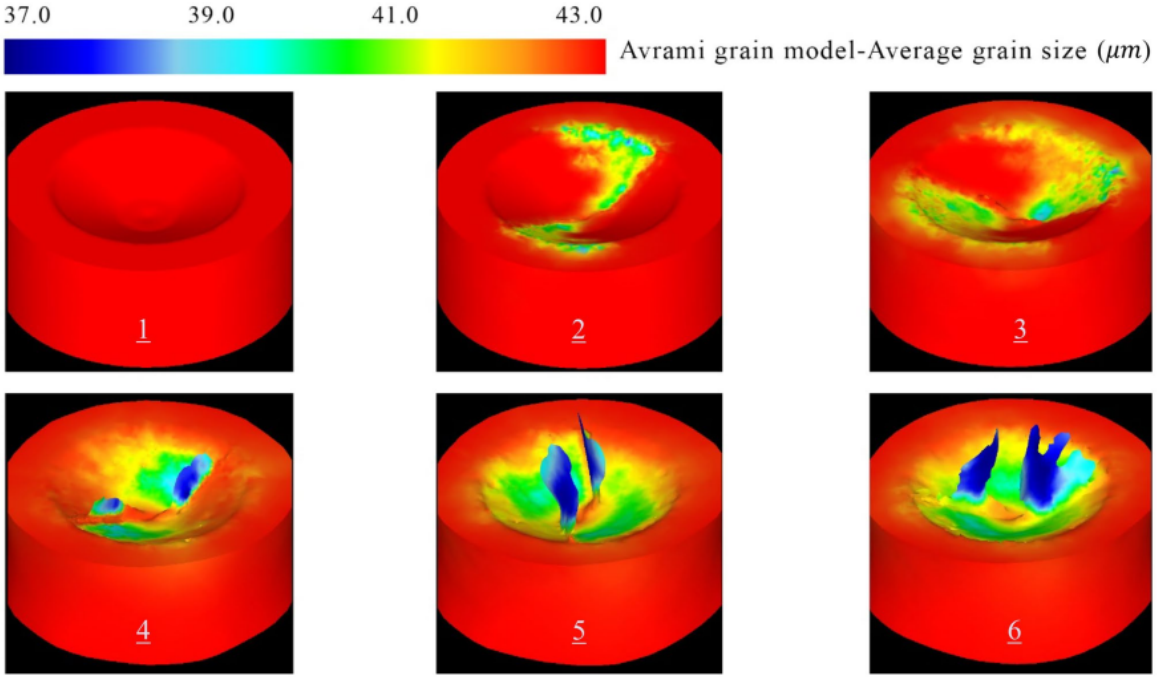


**Fig. 4** The process of microstructure changes during the time in simulation work

The more cutting process goes forward, the more microstructure changes occurred. After the simulation process, the thrust force and average grain size were extracted from the software. To verify the simulation results, the extracted thrust forces were compared by the ones recorded by the dynamometer during the experimental operation.

The full comparison of the thrust force results are given in Fig. 5. It is ascertained from the figure that the predicted results with acceptable errors (less than 10%) are in good agreement with the experimental ones. In most of the run numbers, the predicted values followed the experimental trends. This result shows the utility of the developed

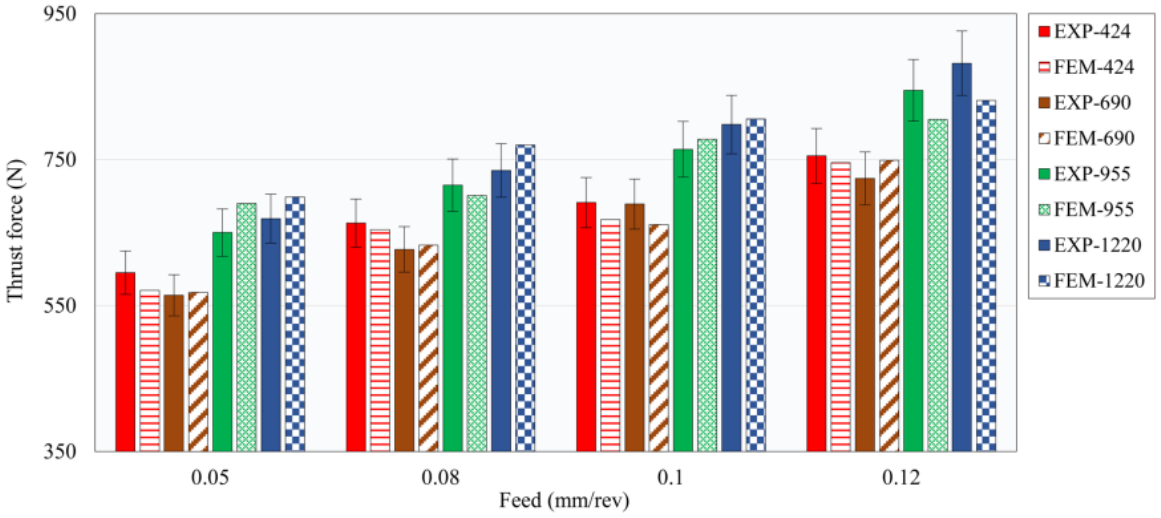


**Fig. 5** Comparison of thrust forces generated in experimental and simulation works

model for further evaluations. Aside from the comparison, it is seen that the variation of cutting parameters influenced the force values. In particular, thrust force increased with an increment in feed value. This could be due to the increase of uncut chip thickness as a result of an increase in feed value. In fact, larger chip thickness caused drill-chip contact length to be increased resulting more force generation during the process [26]. In addition to that, the thrust forces were firstly reduced and then increased by an increase in spindle speed. In general, higher spindle speed causes the thrust force to be reduced in drilling process, due to easier chip shearing phenomenon [27]. But it is somehow different when the workpiece material is a difficult-to-cut material. Owing to the poor thermal conductivity and some special properties of Inconel 718, built-up edge (BUE) phenomenon happened at higher spindle speed. Hence, it causes the sharp of the cutting tool to be rounded thus increasing the cutting forces [27]. BUE was also observed and the discussion is presented in the last section.

### 4.2 Microstructure

Based on the explanations represented in Sect. 2, the metallography operation has been done to reveal the microstructure changes after the drilling process and an example of such micrograph is shown in Fig. 6. It can be seen that a variety of events could have taken place during the drilling process. Severe plastic deformation occurred within 20 $\mu$m under the machined surface causing the orientation of the grains to be changed (in the cutting direction). Furthermore, it is clear that the grains were compressed in this zone and at that instance, white layer is formed which the closest layer to the machined surface. Owing to the resistance of this layer against the etching process, the layer appears in white color under the optical microscope [28]. The white layer is usually introduced as a detrimental layer to the final component which may cause tensile residual stress or a decrease in the strength of bending fatigue [29]. Therefore, post-finishing processes are typically needed in order to remove this layer. It was reported that the formation of white layer is mostly due to high cutting temperature, increment of cutting forces, and deterioration of tool condition during the machining process [29, 30].

Referring to Fig. 7, the thickness of white layer was measured in three points for each particular cutting specimen. Because, this layer is not regular along the cutting edge, therefore, its average is better to be taken into account. Accordingly, the average values of white layers (WL) were reported in Fig. 8, which also shows the microstructure

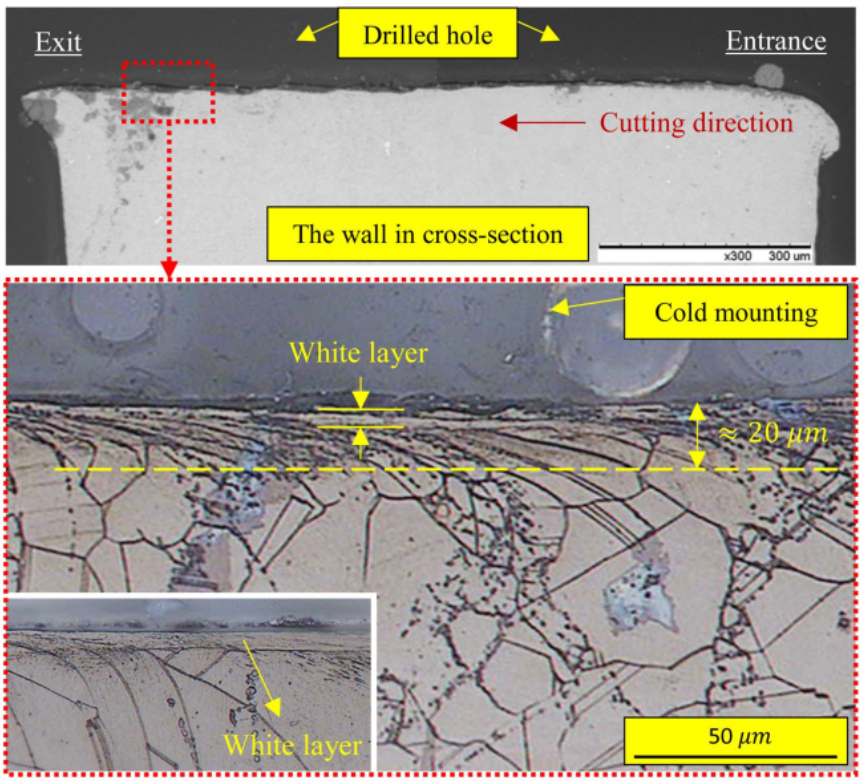


**Fig. 6** Top: drilled hole in cross-section before etching; bottom: the microstructure of drilled hole after etching

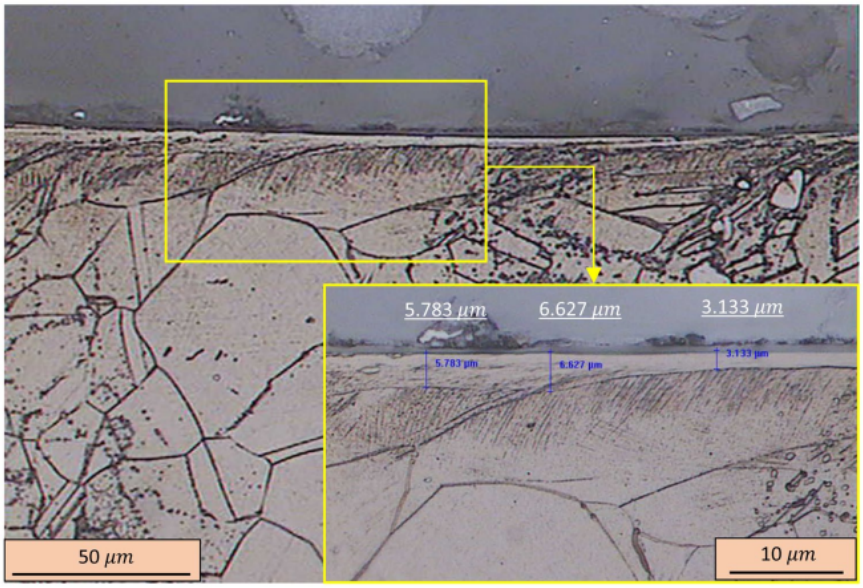


**Fig. 7** White layer measurement after drilling process

changes at different run numbers. The measurement results indicate that the average values of white layers are from 0 to 6 $\mu$m. With respect to Fig. 8, it is evident that the white layer is more prominent in the conditions where the spindle speed and feed rate are at their high levels. This result is compatible with the force result (Sect. 4.1) whereby it was mentioned that cutting forces increased by an increase in cutting parameters. Under low cutting conditions, the white layer was not present or at least it was noncontinuous. This implies that lower cutting forces and lower temperature, decreased the thickness of this layer.

Moreover, in order to investigate the effect of cutting parameters on the grain size, a finite element model was utilized. As mentioned earlier, the experimental results showed that the initial average grain size of Inconel 718 was 43 $\mu$m which was defined as initial value for simulation work. Figure 9 illustrates the chip formation and grain distribution which were observed in Run 7 (feed = 0.1 mm/rev and rotary speed = 690 rpm). It was evident that the drilling process reduced the grain sizes near the drilled surfaces. Note that the experimental average grain size of drilled surfaces were also measured to validate the simulation results. As it is shown in Fig. 6, the grains, which were located near the cutting edge (20 $\mu$m distance from the cutting edge), were selected to measure. Finally, the total results of experiments and simulation works are given in Fig. 10. It is observed that the predicted grain sizes are in good agreement with the experimental ones which was also seen in force comparison. However, one more point can be extracted from grain size comparison. The results show that the FE method could better distinguished between the results. In fact, the experimentally measurement of grain size has typically some errors or it is not as precise as FE method is. Therefore, for instance, it is seen that the experimental result cannot properly distinguish between the microstructure changes in 955 and 1220 rpm. As a result, one of the advantages of using FE method is its precise compared to the experimental measurement.

In accordance with Fig. 10, it was found that the average values of grain sizes are in the range of 37 to 42 $\mu$m. In other words, the grain sizes were reduced about 2 to 14% at different cutting conditions. It was observed that there is not any specific effect of the feed value on the grain size. Meanwhile, the effect of spindle speed variations on the grain size was somehow dependent on the cutting force. It was found that an increase in cutting force, results in reduction in the average grain size. Therefore, it can be concluded that at the highest spindle speed of 1220 rpm, two opposite phenomena occurred at the same time: more creation of white layer and more reduction of grain size. The first phenomenon is not desired as compared to the second one. Hence, better condition was observed when the spindle speed was set at 955 rpm with low feed rate. Under such condition, the white layer and the size of the grain were found to be optimized.

### 4.3 Microhardness

The microhardness measurement was carried out by using a SHIMADZU Vickers pyramid tester where the loading force was set at 4.903 *N* (seen in Fig. 11). The initial hardness of the workpiece material was measured at three points in which the values were: 247.5 *HV*, 249.2 *HV*, and 248.4 *HV*. Furthermore, the hardness of each particular drilled surface was examined in three points in the distance of 40, 120, and 200 $\mu$m from the cutting edge. A schematic of this measurement is shown in Fig. 11.

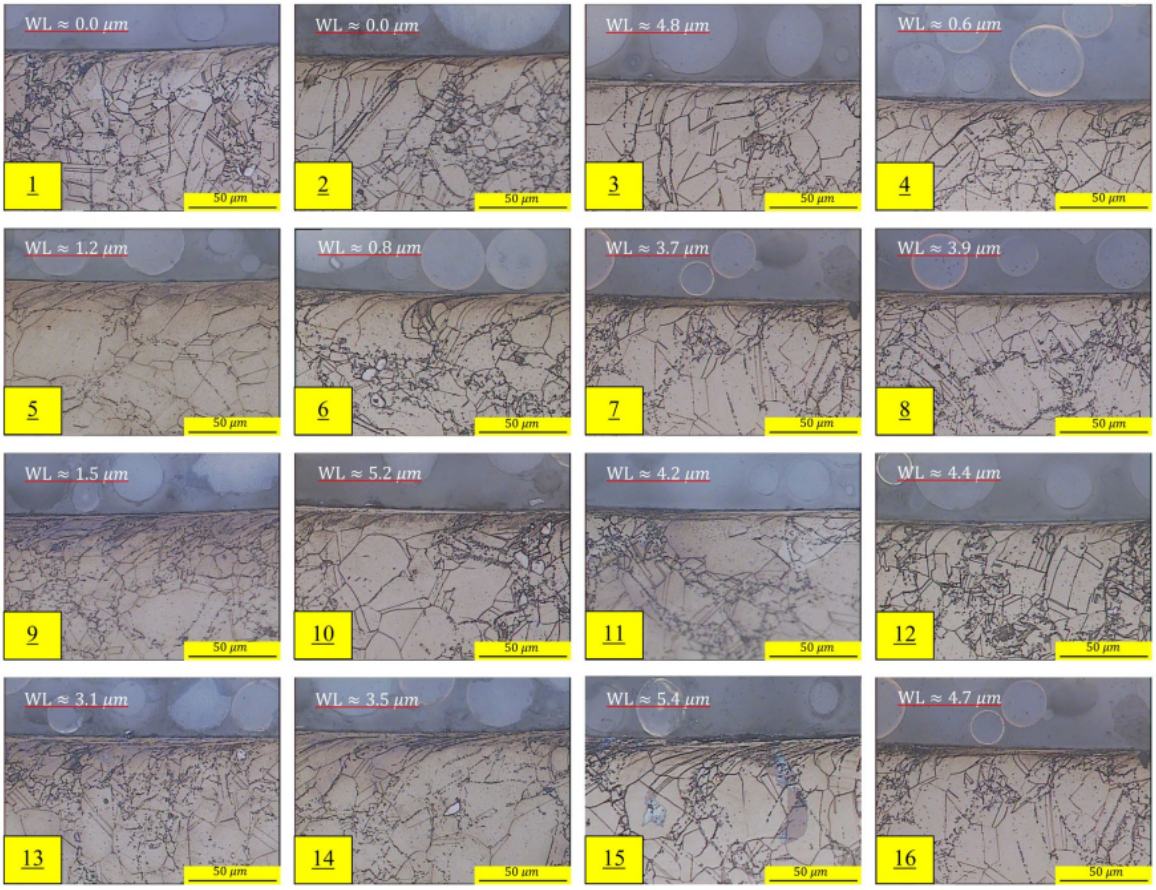


**Fig. 8** Microstructure of drilled holes at different run numbers (1 to 16) plus the average values of the white layer (WL)

The results of microhardness of the specimens after machining process were recorded, as shown in Fig. 12. It was observed that the hardness of drilled surfaces increased compared to the uncut surfaces. This increment was larger at higher spindle speeds. Based on previous studies [28, 29], both white layer and grain size could affect the hardness results. Therefore, the increment of micro-hardness at the highest spindle of 1220 rpm depends on the thicker white layer and smaller grain size created at this condition. The grain size ($d$) effect can be demonstrated by using the Hall-Petch model [31] (Eq. 10):

$$\sigma_o = \sigma_i + \frac{k}{\sqrt{d}} \tag{10}$$

where $k$, $\sigma_o$, and $\sigma_i$ are strengthening coefficient, yield stress, and starting stress of dislocation, respectively. It is observed that a decrement in the grain size increases the microhardness [32].

### 4.4 Surface roughness

Surface roughness is the final parameter of the surface integrity investigated in this study. Three positions of each particular machined surface were measured and then the average values of 16 specimens were compared and presented in Fig. 13. The range of the surface roughness values ($R_a$) were within 0.78 to 1.22 $\mu$m. The surface roughness value increased with an increase in feed rate, due to an increment in the height of feed marks generally produced during the machining process [33, 34], while increment of spindle speed had an inverse effect where it reduced the surface roughness. It could be described by better shearing process that occurred with increment of speed spindle. However,

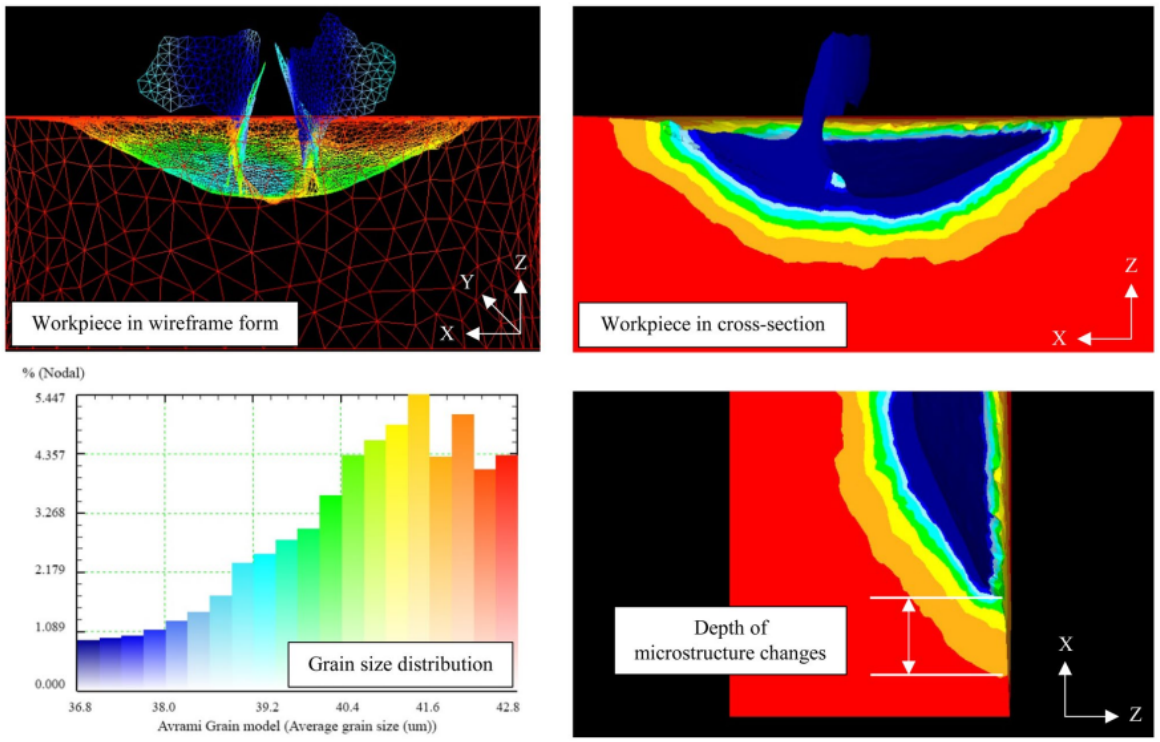


**Fig. 9** Simulated grain size distribution

this improvement was stopped at the highest level of this parameter.

One major problem in machining of Inconel 718 is the generation of BUE at higher spindle speeds as shown in Fig. 14. Under this condition, the temperature increases and the deformed chip periodically sticks on the drill bit and machined surfaces [35]. It caused an increase in surface roughness values at highest level of spindle speed (1220 rpm).

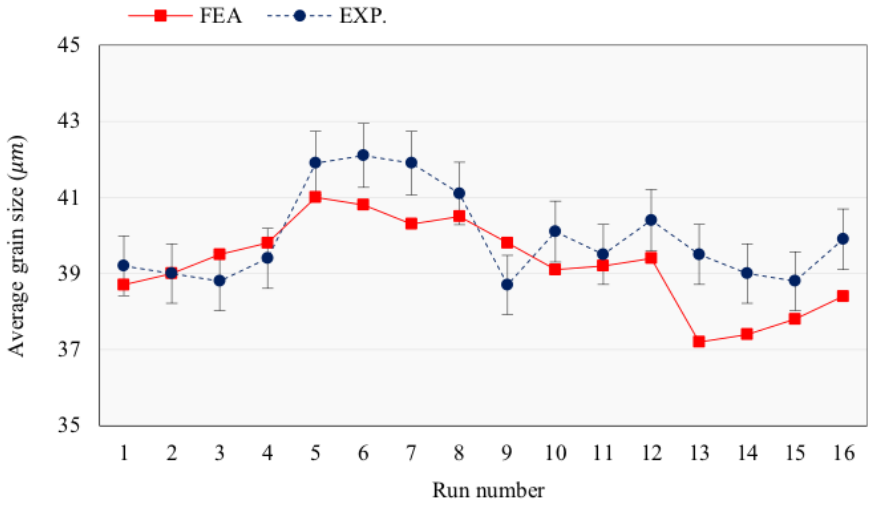


**Fig. 10** Comparison of experimental and estimated average grain sizes at different run numbers

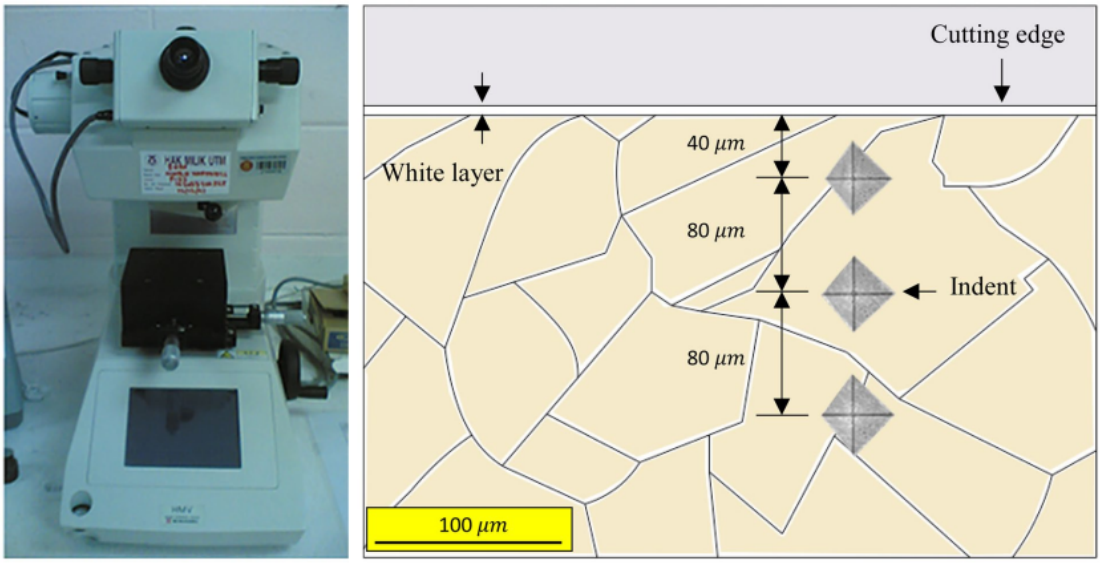


**Fig. 11** Microhardness measurement device and a schematic figure to indicate the location of indentations

**Fig. 12** Measurement results of microhardness

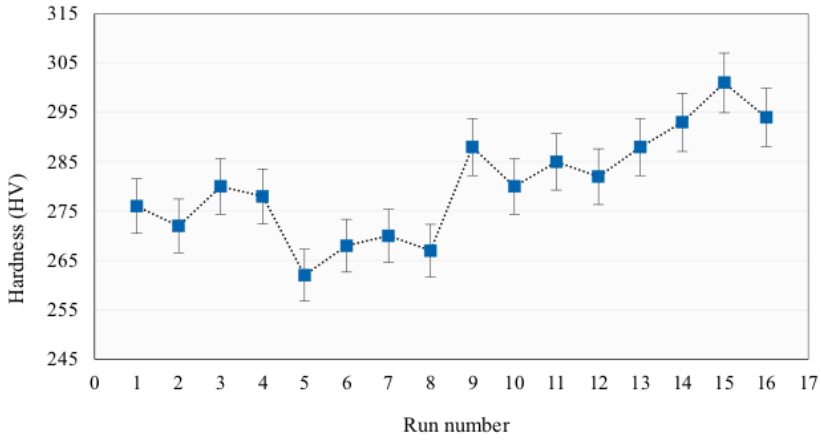


**Fig. 13** Measurement results of surface roughness ($R_a$)

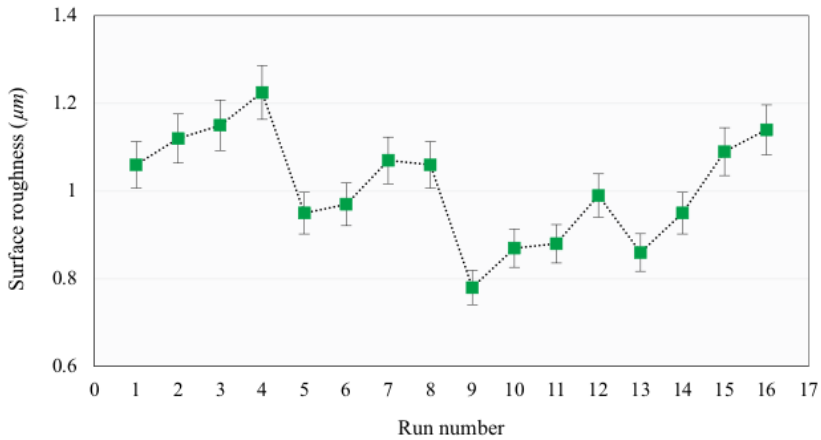

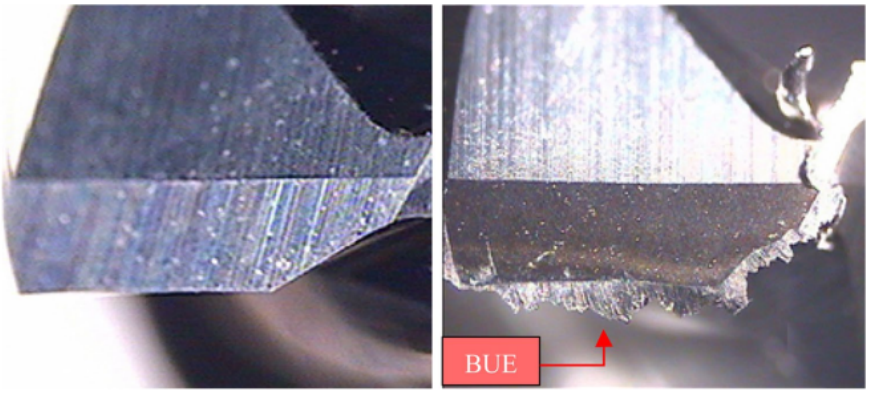


**Fig. 14** Left: new tool; right: tool with built-up edge

## 5 Conclusions

In this study, the experimental trials and simulation modeling method were used to investigate the effect of different cutting parameters on surface integrity which includes microstructure changes, grain size, microhardness, and surface roughness when drilling Inconel 718 by using carbide tool. Based on the results, the following conclusions are drawn:

1. Evaluation of metallography results showed that severe plastic deformation and white layer were generated near the machined surfaces. It was found that lower cutting forces (at low levels of cutting parameters) caused the thickness of white layer to be reduced.
2. The simulated and the experimental average grain sizes indicated that the drilling process reduced the grain sizes from 2 to 14% at different cutting conditions. It was found that an increase in the cutting forces reduced the average grain size of the microstructure. In fact, more creation of white layer and more reduction of grain size were observed at the highest spindle speed of 1220 rpm which resulted in an increase in microhardness value.
3. In general, increment of spindle speed reduced the surface roughness values. However, the roughness values increased at the highest level of cutting conditions due to the effect of BUE.
4. In this study, the desired condition was that the grain size, the thickness of the white layer, and the surface roughness to be reduced and the microhardness increases. Accordingly, it was found that an increase in spindle speed tends to improve the microhardness and the grain size; however, it deteriorates the surface roughness (at its highest level) and worsen the white layer formation. Surface roughness and white layer could more deteriorate with an increase in feed value. Therefore, based on the experimental and simulation results, it can be suggested that the best condition when drilling of Inconel 718 in order to obtain an acceptable surface integrity is to employ the medium spindle speed (955 rpm) and low level of feed rate (0.05 mm/rev).

**Author contribution** Mohammad Lotfi: conceptualization, methodology, resources, writing—original draft. Ali Akhavan Farid: conceptualization, methodology, experimental tests. Javad Akbari: supervision and editing. Safian Sharif: supervision and editing. Amrifan Saladin Mohruni: experimental tests.

**Funding** The authors wish to thank Sharif University of Technology, University of Nottingham Malaysia Campus, and Universiti Teknologi Malaysia for their cooperation and assistance throughout conducting this research. Special appreciation to the Iran National Science Foundation (INSF) and Iran's National Elites Foundation (INEF) for the financial support through the Shahid Chamran Post-Doctoral Grant of 99010445 and also to the Research Management Centre of UTM for the financial support through the research funding's of 4B390 and 04G39.

**Availability of data and materials** All data generated or analyzed during this study are included in this published article (and its supplementary information files).

## Declarations

**Ethical approval** Our paper is an original paper which has neither previously, nor simultaneously, in whole or in part been submitted anywhere else. All authors prove that the paper is an original paper.

**Consent to participate** The authors agreed to participate in this manuscript.

**Consent to publish** The authors agreed with this submission.

**Conflict of interest** The authors declare no competing interests.

## References

1. Khanafer K, Eltaggaz A, Deiab I, Agarwal H, Abdul-Latif A (2020) Toward sustainable micro-drilling of Inconel 718 superalloy using MQL-Nanofluid. Int J Adv Manuf Technol 1–11

2. Uçak N, Çiçek A (2018) The effects of cutting conditions on cutting temperature and hole quality in drilling of Inconel 718 using solid carbide drills. J Manuf Process 31:662–673
3. Lotfi M, Amini S, Sajjady SA, Juaifer AH (2018) The effectiveness of ceramic wiper tool in turning of Monel K500. J Modern Process Manuf Prod 7(2):47–64
4. Khanna N, Agrawal C, Gupta MK, Song Q (2020) Tool wear and hole quality evaluation in cryogenic drilling of Inconel 718 superalloy. Tribol Int 143:106084
5. Lotfi M, Farid AA, Jahanbakhsh M (2019) Tool wear deceleration in turning of Inconel 625. Int J Mach Mach Mater 21(4):321–335
6. Sharman ARC, Hughes JI, Ridgway K (2015) The effect of tool nose radius on surface integrity and residual stresses when turning Inconel 718™. J Mater Process Technol 216:123–132
7. Lotfi M, Amini S, Aghayar Z, Sajjady SA, Farid AA (2020) Effect of 3D elliptical ultrasonic assisted boring on surface integrity. Measurement 108008
8. Azim S, Gangopadhyay S, Mahapatra SS, Mittal RK, Singh A, Singh RK (2019) Study of cutting forces and surface integrity in micro drilling of a Ni-based superalloy. J Manuf Process 45:368–378
9. Sharman ARC, Amarasinghe A, Ridgway K (2008) Tool life and surface integrity aspects when drilling and hole making in Inconel 718. J Mater Process Technol 200(1–3):424–432
10. Yin Q, Liu Z, Wang B, Song Q, Cai Y (2020) Recent progress of machinability and surface integrity for mechanical machining Inconel 718: a review. Int J Adv Manufact Technol 1–31
11. Liang X, Liu Z, Wang B (2019) State-of-the-art of surface integrity induced by tool wear effects in machining process of titanium and nickel alloys: A review. Measurement 132:150–181
12. Rotella G, Umbrello D (2014) Finite element modeling of microstructural changes in dry and cryogenic cutting of Ti6Al4V alloy. CIRP Ann 63(1):69–72
13. Jafarian F, Umbrello D, Jabbaripour B (2016) Identification of new material model for machining simulation of Inconel 718 alloy and the effect of tool edge geometry on microstructure changes. Simul Model Pract Theor 66:273–284
14. Denguir LA, Outeiro JC, Fromentin G, Vignal V, Besnard R (2016) Orthogonal cutting simulation of OFHC copper using a new constitutive model considering the state of stress and the microstructure effects. Procedia cIRP 46:238–241
15. Ding H, Shin YC (2013) Multi-physics modeling and simulations of surface microstructure alteration in hard turning. J Mater Process Technol 213(6):877–886
16. Arısoy YM, Özel T (2015) Prediction of machining induced microstructure in Ti–6Al–4V alloy using 3-D FE-based simulations: Effects of tool micro-geometry, coating and cutting conditions. J Mater Process Technol 220:1–26
17. Arısoy YM, Guo C, Kaftanoğlu B, Özel T (2016) Investigations on microstructural changes in machining of Inconel 100 alloy using face turning experiments and 3D finite element simulations. Int J Mech Sci 107:80–92
18. Bai W, Sun R, Leopold J, Silberschmidt VV (2017) Microstructural evolution of Ti6Al4V in ultrasonically assisted cutting: Numerical modelling and experimental analysis. Ultrasonics 78:70–82
19. Lotfi M, Amini S, Akbari J (2020) Surface integrity and microstructure changes in 3D elliptical ultrasonic assisted turning of Ti–6Al–4V: FEM and experimental examination. Tribol Int 151:106492
20. Deform® user manual. Columbus, OH, USA: SFTC-Deform; 2014. https://toaz.info/doc-viewer
21. Lotfi M, Amini S, Sajjady SA (2019) Development of a friction model based on oblique cutting theory. Int J Mech Sci 160:241–254
22. Yadav RK, Abhishek K, Mahapatra SS (2015) A simulation approach for estimating flank wear and material removal rate in turning of Inconel 718. Simul Model Pract Theor 52:1–14
23. Thepsonthi T, Özel T (2016) Simulation of serrated chip formation in micro-milling of titanium alloy Ti-6Al-4V using 2D elasto-viscoplastic finite element modeling. Prod Eng 10(6):575–586
24. Thepsonthi T, Özel, T (2015) 3-D finite element process simulation of micro-end milling Ti-6Al-4V titanium alloy: experimental validations on chip flow and tool wear. J Mater Process Technol 221:128–145
25. Özel T, Arısoy YM, Guo C (2016) Identification of microstructural model parameters for 3D finite element simulation of machining Inconel 100 alloy. Procedia CIRP 46:549–554
26. Amini S, Alinaghian I, Lotfi M, Teimouri R, Alinaghian M (2017) Modified drilling process of AISI 1045 steel: a hybrid optimization. Eng Sci Technol Int J 20(6):1653–1661
27. Lotfi M, Amini S, Al-Awady IY (2018) 3D numerical analysis of drilling process: heat, wear, and built-up edge. Adv Manuf 6(2):204–214
28. Badin V, Badin CRB, Machado AR, Amorim FL (2020) Machining of Inconel 718 with a defined geometry tool or by electrical discharge machining. J Braz Soc Mech Sci Eng 42(5)
29. Tonshoff H, Wobker HG, Brandt D (1995) Tribological aspects of hard turning: influence on the workpiece properties. Trans NAMRI SME 23
30. Wang B, Liu Z, Cai Y, Luo X, Ma H, Song Q, Xiong Z (2021) Advancements in material removal mechanism and surface integrity of high speed metal cutting: a review. I J Mach Tools Manuf 103744
31. Smith WF, Hashemi J, Presuel-Moreno F (2006) Foundations of materials science and engineering. Mcgraw-Hill Publishing
32. Jafarian F, Ciaran MI, Umbrello D, Arrazola PJ, Filice L, Amirabadi H (2014) Finite element simulation of machining Inconel 718 alloy including microstructure changes. Int J Mech Sci 88:110–121
33. Lotfi M, Amini S (2019) Effect of longitudinally intermittent movement of cutting tool in drilling of AISI 1045 steel: A three-dimensional numerical simulation. Proc Ins Mech Eng Part C J Mech Eng Sci 233(12):4081–4090
34. Lotfi M, Akbari J (2021) Finite element simulation of ultrasonic-assisted machining: a review. Int J Adv Manuf Technol 1–20
35. Khadtare A, Pawade R, Varghese A, Joshi S (2020) Micro-drilling of straight and inclined holes on thermal barrier coated Inconel 718 for turbine blade cooling. Mater Manuf Process 1–14

# Evaluation of surface integrity when drilling Inconel 718 through experimental measurement and finite element analysis

ORIGINALITY REPORT

8%
SIMILARITY INDEX

MATCHED SOURCE

| | | |
|---|---|---|
| 1 | "Proceedings of the 37th International MATADOR Conference", Springer Science and Business Media LLC, 2013<br>Crossref | 93 words — 2% |

★"Proceedings of the 37th International MATADOR Conference", Springer Science and Business Media LLC, 2013 — 2%
Crossref

| | | | |
|---|---|---|---|
| EXCLUDE QUOTES | OFF | EXCLUDE SOURCES | < 1% |
| EXCLUDE BIBLIOGRAPHY | ON | EXCLUDE MATCHES | OFF |